Universidad Zaragoza
1542

Final Master Project

Synthesis and characterization of electrospun oxide fibers for catalytic applications

Author

Jorge Sebastián Coba Daza

Director

Dr. Silvia Irusta Alderete

NANOSTRUCTURED MATERIALS FOR NANOTECHNOLOGICAL APPLICATIONS
Institute of Nanoscience of Aragon
University of Zaragoza
2018-2019

Acknowledgements

I would like to express my deep gratitude to my supervisor Dr Silvia Irusta, for their patient guidance and useful critiques of this research work together with the XPS analysis. I'm grateful to have had the opportunity to work on the Nanoporous films and particles (NFP) research group.

I would also like to thank to Fundación Carolina for the support and the scholarship during all the master, and all my classmates and the people who help me to finishing this work on time, to Guillermo Landa for tech me the use of the electrospinning equipment, to Nuria Navascues for her help in the XRD and TGA analysis, to Victor Sebastian for their help making the TEM and to Martín Prieto to tech me how to use the MP-AES. Thank you.

Last, but not least, I want to thank to my mom, without her continuous support in the distance, I couldn't have been able to finish this work. I love you.

Table of Contents

Table of figures

Tables

Abstract

Electrospinning is a versatile technique that uses an electrical charge to produce very fine fibers from a polymeric solution. It has very high potential to be applied in different fields as in energy storage, in medicine, in cosmetics and in catalysis. Electrospinning is cost effective, reproducible and it can produce long and continuous nanofibers. Polymers such polyamides, polyalcohol and PVP among others, can be easily electrospun. The use of inorganic nanofibers obtained from template-based electrospun polymers is increasing because their performance in different applications due to the high surface to volume ratio.

In this work three different nanofibers (Ce_2O/NiO, CeO_2/NiO/MgO and TiO_2-doped-Fe_2O_3 NP) were synthesized trough electrospinning process followed by a calcination process. The processing conditions such as voltage applied and feed rate in the electrospinning process were studied to find the best conditions for uniform fibers production. The calcination process was performed to completely oxidize the organic PVP present and promote the growth of the oxide nanoparticles that form the nanofiber.

Characterization techniques such as scanning electron microscopy (SEM), energy dispersive X-ray spectroscopy (EDX), transmission electron microscopy (TEM), X-ray diffraction (XRD), X-ray photoelectron spectroscopy (XPS), thermogravimetric analysis (TGA), microwave plasma-atomic emission spectroscopy (MP-AES), temperature programmed reduction (TPR), dynamic light scattering (DLS) and UV-vis spectroscopy were used to study the morphology, chemical and crystal characteristics of the samples. This work discusses the possibility to future use of the different synthesized nanofibers in the applications in catalysis for the CO_2 methanation reaction (CeO_2/NiO and CeO_2/NiO/MgO nanofibers) and the water pollutants removal (TiO_2-dop-Fe_2O_3 NP).

Keywords

Electrospinning, inorganic nanofibers, physicochemical characterization, catalysis.

1. Introduction

One-dimensional nanomaterials are structures with at least one size in the nanoscale (<100 nm), this characteristic provides different interesting properties comparing to the bulk material [1], which makes them very attractive in applications fields as energy devices [2], bioengineering [3], environmental engineering [4] and so forth. Nanosheets, nanotubes, nanocables, and nanofibers are examples of 1D-materials present in many fields [5]. Nowadays exist many routes of synthesis (chemical-based and physical-based) of those nanomaterials that can produce the desired final characteristics like the dimensions, the shape and even the physico-chemical properties [6]. Regarding nanofibers as one of the most important 1D-nanomaterial, researchers are improving considerably in the preparation methods as well as the control of the purity degree and the size [5].

Since the beginning of the use of electrospinning, as the main process for the nanofibers production, increased number of researchers have been used this versatile technique to understand the theoretical and practical aspects of their production as well as the characteristics of the resultant fibers with the help of theoretical models and experimental characterization [7]–[9], nevertheless, exist some conditions and materials whereby it is necessary to keep studying in detail.

Regarding electrospinning, it is a technique that consist in the application of an electrical field between two electrodes, the needle and the collector, as it is shown in the schematic representation of the process (Figure 1). When the applied voltage increase, a charge is induced in the drop of the ejecting polymer solution, changing the surface tension and consequently changing the shape of the drop from hemispherical to conical [10, 12]. This conical shape of the ejected solution is commonly referred as Taylor cone [13]. To obtain the desire characteristics of the electrospun nanofiber, many parameters must be considered. Those parameters are characterized into three main groups, the solution parameters, the process parameters and the ambient parameters [13].

Solution parameters implies the physical properties of the fluid, as the solvent and polymer used, the surface tension, the viscosity, the polymer molecular weight and the solution

conductivity, those parameters greatly influence the electrospinning process and the obtained morphology of the nanofibers [13]. The other important parameters are referred to the processing conditions such as external voltage, feed rate, collector plate and the distance between source and collector that should be optimized. Finally, the ambient parameters play a crucial role as well, the humidity and the temperature could change the final behaviour of the nanofibers, it is important then to keep them under control [14, 15].

In this kind of process, it is possible to process both, natural and synthetic polymers, to fabricate nanofibers, as well as processing mixtures of polymers, in order to obtain different type of fibers [16]. The applications of such fibers goes from filtration, drug delivery systems, sensors, optical materials and even in catalysis [17]–[20].

Inorganic fibers can be also obtained by the electrospinning technique [21]. Typically, inorganic precursors are mixed with a polymer solution for electrospinning, once the fibers are fabricated, they have to go through a calcination process which allows all the organic material get removed. Sintering parameters such as temperature and heating rate are crucial in the final product regarding form and crystalline phase [4]. Indeed, the fibers undergo three main steps during the calcination process. The first step involves the removal of the residual water vapour and solvents from the nanofibers [22], the second one is when all the organic material is removed allowing the condensation and structural relaxation proceed [21], the final step depends on the material and the temperature, and is related with the glass transition stage; nevertheless, in most of the cases the formation of inorganic fibers ends at the step number two [21].

Inorganic fibers have been used in many applications such as electrodes for sensors [23], solar cells dyes [24], and in the catalysis field [25, 26]. The inorganic fibers of some metal oxides (TiO_2, ZnO, CeO_2, NiO, MgO) are used to minimize the activation energy in various reactions as the production of methane from CO_2 [27]. Hydrogenation of carbon dioxide (CO_2) for the production of fuels, have been studied as an alternative for the reduction of the greenhouse emissions, in particular, nickel-based and nickel-magnesium-based catalysts supported on different metal oxides (e. g. CeO_2) are used for this purpose. Different morphologies were studied, and the nanofibers represent a great alternative due the high surface to volume ratio showing high selective and space-time yield comparing to bulk and

even to other morphologies [26, 28]. Also, taking advantage of the photocatalytic properties of TiO_2, nanofibers have demonstrated an adequate performance in water pollutants removal [29-30], however, there is a persistent problem in the separation and recovery of the catalyst from large water volumes, which increase the cost. To solve this problem the incorporation of magnetic nanoparticles, especially iron oxides, are being used to magnetically remove them from water [31]. Beside, by the addition of ferric nanoparticles the absorption properties are shifted to the visible light range, bringing an interesting opportunity to their use in catalysis [32].

In this work three different inorganic fibers were synthesized by electrospinning. The physicochemical properties of the materials were analysed trough different characterization techniques as SEM, TEM, XPS, TGA, TPR and MP-AES. In a future work the obtained fibers of CeO_2/NiO and CeO_2/NiO/MgO will be used as catalysts for CO_2 hydrogenation while the TiO_2 nanofibers doped with Fe_2O_3 nanoparticles will be tested in the photocatalytic removal of organic compounds in water.

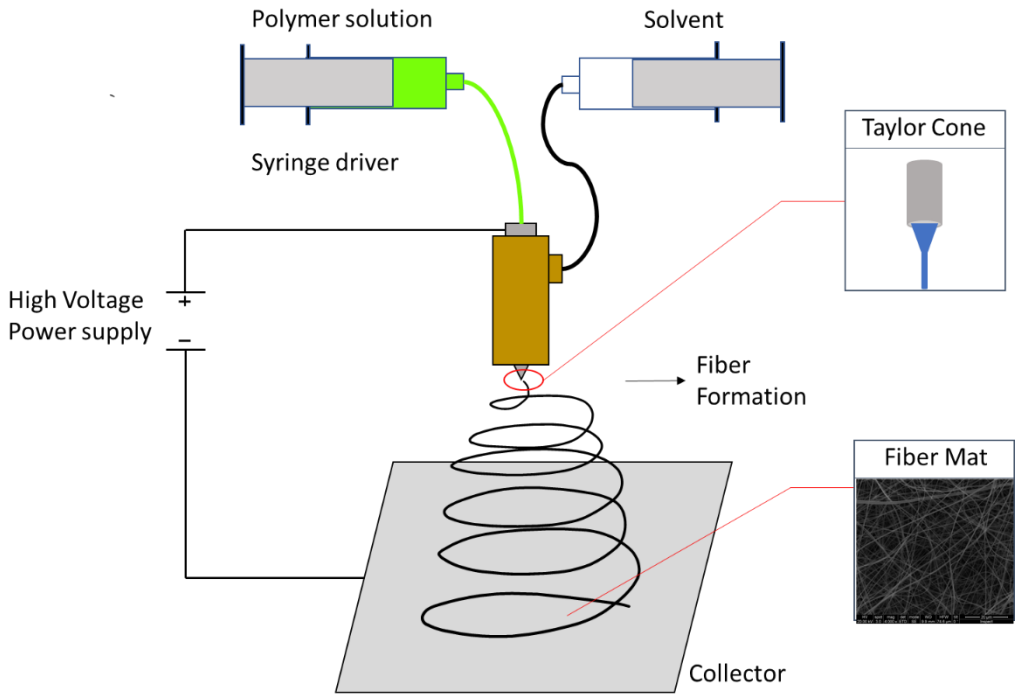

Figure 1: Graphical representation of the electrospinning process with coaxial solvent incorporation

2. Objectives

The main goal of this final master project was to obtain three different inorganic nanofibers such as CeO_2/NiO, CeO_2/NiO/MgO and TiO_2-doped-Fe_2O_3 nanoparticles and perform its respective characterization. The main tasks to be accomplished during the project to achieve this objective were:

- Optimization of the electrospinning parameters (voltage, flow rate, tip-to-collector distance) to obtain bead-free, uniform fibers.
- Optimization of the calcination conditions for the complete elimination of the polymer.
- Characterization by different techniques (SEM; EDX; TEM; XRD; XPS; TGA; MP-AES; TPR; DLS; UV-vis spectroscopy) to confirm the morphology, chemical and crystallographic nature of the produced fibers.

3. Experimental methods

3.1. Materials

The following reagents were used in order to prepare the different nanofibers: Cerium nitrate hexahydrate $Ce(NO_3)_3 \cdot 6H_2O$, nickel nitrate hexahydrate ($Ni(NO_3)_2 \cdot 6H_2O$), magnesium nitrate hexahydrate ($Mg(NO_3)_3 \cdot 6H_2O$), polyvinylpyrrolidone (PVP, Mw 1300000), titanium IV isopropoxide ($Ti[OCH(CH_3)_2]_4$), acetic acid (CH_3COOH), absolute ethanol (C_2H_5OH) and deionized water (H_2O) all from Sigma Aldrich.

3.2. Production of inorganic nanofibers

3.2.1. CeO_2/NiO nanofibers

To prepare CeO_2/NiO nanofibers with a nominal content of 15 at % Ni, 0.622 g of cerium nitrate ($Ce(NO_3)_3 \cdot 6H_2O$) and 0.106 g of nickel nitrate ($Ni(NO_3)_2 \cdot 6H_2O$) were dissolved in a mixture of 10 mL of ethanol and 2 mL of water under magnetic stirring. Then 1 g of PVP was added to the solution keeping the magnetic stirring overnight to ensure the complete dissolution. A coaxial setup for the electrospinning was used, the prepared solution was fed to the inner needle while ethanol was flowing for the external one. The flow rates for the inner and the external solutions were 1 mL/h and 0.2 mL/h respectively. The distance between the needle and the collector was 25 cm and +9 kV were applied in the positive electrode (connected to the needle) and -2 kV to the negative electrode (connected to the collector). The obtained fibers were calcinated in a muffle furnace (OBERSAL). The calcination process was performed at 550°C during 6 h with a heating rate of 0.5°C/min.

3.2.2. CeO_2/NiO/MgO nanofibers

A very similar process to produce CeO_2/NiO/MgO nanofibers was implemented, in this case, to achieve a concentration of 20 at.% of Ni in the fibers and with equal amount of Ce and Mg. For this, 0.319 g of cerium nitrate ($Ce(NO_3)_3 \cdot 6H_2O$), 0.1835 g of magnesium nitrate ($Mg(NO_3)_3 \cdot 6H_2O$) and 0.106 g of nickel nitrate ($Ni(NO_3)_2 \cdot 6H_2O$) were weighted and dissolved in 10 mL of ethanol and 2 mL of water together with 1 g of PVP, the solution was kept overnight under magnetic stirring. The parameters for the electrospinning process were +10/-3 kV of applied voltage, 1 mL/h and 0.2 mL/h of feed rates for the inner and external

solution respectively and 25 cm of needle-collector distance. Same calcination parameters as in CeO_2/NiO nanofibers were used to completely remove the polymer.

3.2.3. TiO_2 nanofibers doped with Fe_2O_3 nanoparticles

Sol-gel method was used in order to prepare the TiO_2 nanofibers. Two solutions were prepared, the solution number 1 contains 0.5 g of PVP in 10 mL of ethanol, the solution was prepared under magnetic stirring during overnight to ensure the complete dissolution. Then 39.5 mg of Fe_2O_3 nanoparticles, synthesized by 'Zeolitas' group from the Universidad Tecnologica Nacional, Facultad Regional Cordoba, Argentina, were added in order to have 6 wt.% (9% mol) with respect to the total nanofiber. The solution number 2 was made of 5 mL of ethanol, 3 mL of acetic acid and 1.5 g of titanium IV isopropoxide ($Ti[OCH(CH_3)_2]_4$). Finally, solution 2 was added drop by drop to solution 1 under constant magnetic stirring for 30 minutes. A coaxial setup was used again to fabricate the TiO_2 nanofibers doped with Fe_2O_3 nanoparticles. The flow rates for the inner and the external solutions were 1 mL/h and 0.1 mL/h respectively. Collector distance and applied voltage were 15 cm and +10/-5 kV, respectively. Finally, a calcination process was performed at a temperature of 550°C for 6 h with a heating rate of 0.5 °C/min.to obtain the inorganic fibers.

3.3. Characterization

3.3.1. Scanning electron microscopy (SEM)/Energy dispersive X-ray spectroscopy (EDS)

Morphological and semiquantitative chemical composition for the fibers were studied with scanning electron microscopy (INSPECT-F50) and X-ray spectroscopy (EDX detector). The samples were metallized with thin layer of carbon on top in a Sputter Coater SC7620 (Quorum Technologies). Diameter size distribution of all the synthesized nanofibers (n=100) were measured with ImageJ software 1.47V (NIH, USA).

3.3.2. Transmission electron microscopy (TEM)

A solution of each calcined nanofiber was dispersed in ethanol, then a drop of each one was placed in the TEM grids, and let the solvent evaporate. The samples were analysed by transmission electron microscopy (TEM) using a Tecnai F30, FEI, operated a 300 kV (USLMA INA-UNIZAR).

3.3.3. X-Ray diffraction (XRD)

The X-ray powder diffraction for the calcined nanofibers was carry out in a D-Max Rigaku, Ru300 diffractometer with a rotating Cu anode and a graphite monochromator to select the CuKα radiation from 20° to 120° 2θ degrees for CeO_2/NiO nanofibers and CeO_2/NiO/MgO nanofibers, and from 5° to 90° in the case of TiO_2 nanofibers doped with Fe_2O_3 nanoparticles with a scanning rate of 0.03°/s.

3.3.4. X-ray photoelectron spectroscopy (XPS)

The X-ray photoelectron analysis (XPS) was performed with an Axis SUPRA DLD (Kratos Tech.). The spectra were excited by a monochromatized AlKα source (1486.6 e.V) run at 15 kV and 10 mA. The binding energies were referenced to the internal C 1s (285.0 eV) standard.

3.3.5. Thermo gravimetric analysis (TGA)

In order to check that the polymer elimination was complete, a thermogravimetric analysis with a Mettler Toledo TGA/STDA 851 was done. The calcinated fibers were analysed in a temperature range from 25°C up to 900°C with a rate of 5°C/min using 50 mL/min of synthetic air as purge gas.

3.3.6. Microwave plasma – atomic emission spectrometry (MP-AES)

To quantify the amount of cerium and nickel in the nanofibers a microwave plasma- atomic emission spectroscopy equipment (MP-AES 4100) was used. The samples were digested in aqua regia, then water was added in order to achieve a concentration of 1 ppm. Also, a calibration curve was done in order to calculate the concentration of each element in the samples, for that, Ce and Ni patterns from Fluka® analytical were diluted sequentially to a concentration of 10, 8, 5, 2 and 1 ppm. Both, sample and pattern (calibration curve), were measured by triplicate using three lines of different wavelengths, according to the atomic emission for the elements.

3.3.7. Temperature programmed reduction (TPR)

Reducibility of the CeO_2/NiO nanofibers was studied by temperature-programmed-reduction. Measurements were carried out in an AutoChem II 2920 (Micrometrics) with a temperature range of 25–900 °C and a heating rate of 10 °C min^{-1}. The mass of the sample in each test was ca. 50 mg. The investigated materials were reduced in a mixture of 10% H_2–

90% Ar with a volumetric flow rate of 20 mL/min. Hydrogen consumption was measured with a thermal conductivity detector (TCD).

3.3.8. Dynamic light scattering (DLS)

Fe_2O_3 nanoparticles were dispersed in water followed by ultrasound bath during 15 min. Well dispersed samples were analysed through Brookhaven 90Plus Particle Size Analyzer in order to find the particle size distribution.

3.3.9. UV-Vis spectroscopy

The absorption properties of the TiO_2 nanofibers doped with Fe_2O_3 nanoparticles were analysed through UV-visible diffuse reflectance in a spectrophotometer of the type Jasco V-670 in a wavelength interval from 200 nm to 800 nm.

4. Results and discussions

4.1. CeO_2/NiO nanofibers

Different applied voltage and feed rate were tested in order to find the best conditions in which the Taylor cone was stable, thus producing the nanofibers. Table 1 shows three different conditions tested. Increasing the applied voltage and reducing the feed rate (with collector-needle and solution concentration constants), the stability of the Taylor cone can be increased allowing to the proper formation of the nanofibers. It is known [32, 33] the influence of those parameters in the production of the nanofibers and its diameter. Generally, as the applied voltage increase, the nanofiber's uniformity increase, and the diameter decrease, this is attributed to the stretching of the polymer jet related with the charge repulsion [34]. Feed rate is other critical parameter that define the final characteristics of the nanofiber, the formation of beads is generally attributed to the increment of the feed rate. Keeping the minimum possible value of the feed rate in where the Taylor's cone is stable, allows the formation of bead-free nanofibers [35].

Table 1: Used parameters to find the best conditions to nanofibers fabrication

Condition	Applied voltage (kV)	Feed rate external needle (mL/h)	Distance (cm)	Comments
1	+5/-2	3	25	Instable cone, no fibers production.
2	+7/-2	2	25	Instable cone, irregular shape nanofibers.
3	+9/-2	1	25	Stable cone and good production of fibers

SEM was employed to investigate the general morphology of the nanofibers. By the one hand, it was possible to identify bead-like structures with the condition number 2 presented in the Table 1. Figure 2 show the obtained irregular bead-like fibers, those kinds of fibers are classified as fewer quality nanofibers, and therefore the parameters should be changed in order to obtain the bead-free nanofibers. Changing the condition from 2 to 3 (Table 1), it was

possible to obtain a good quality nanofibers to be used as a template for the inorganic fibers fabrication through the calcination process.

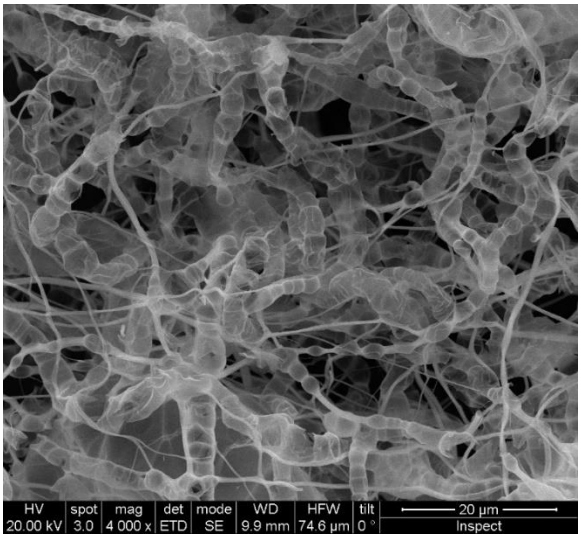

Figure 2: Obtained beads-like fibers with the condition number 2.

About the calcination process, different times of procedure were tested in order to find the condition where the organic material (PVP) get completely remove of the sample. By varying the time from 4 to 6 h it was possible to observe homogeneity of the sample by SEM analysis. The 4 h time of calcination produced two kind of morphologies in the sample, one identically to the un-calcinated fibers and the other the typical morphology in found in the calcinated nanofibers. By increasing this temperature to 6 h, it was observed the homogeneity of the morphology across the sample.

Figure 3 shows the CeO_2/NiO nanofibers obtained with the best parameters before and after calcination. The as-prepared nanofibers presented an uniform size distribution with average diameter of 305 ±71 nm (inset Figure 3(A)), whereas the calcined CeO_2/NiO fibers showed an average diameter of 113 ± 30 nm (inset Figure 3(B)). This decreasing in the diameter can be attributed to the elimination of the PVP organic matrix during the oxidative calcination process. In order to confirm the success of the calcination process a thermogravimetric analysis (TGA) was performed on the calcinated nanofibers. No significative changes in the sample weight was observed along the temperature range evaluated (25–900 °C), demonstrating the complete removal of the organic PVP matrix.

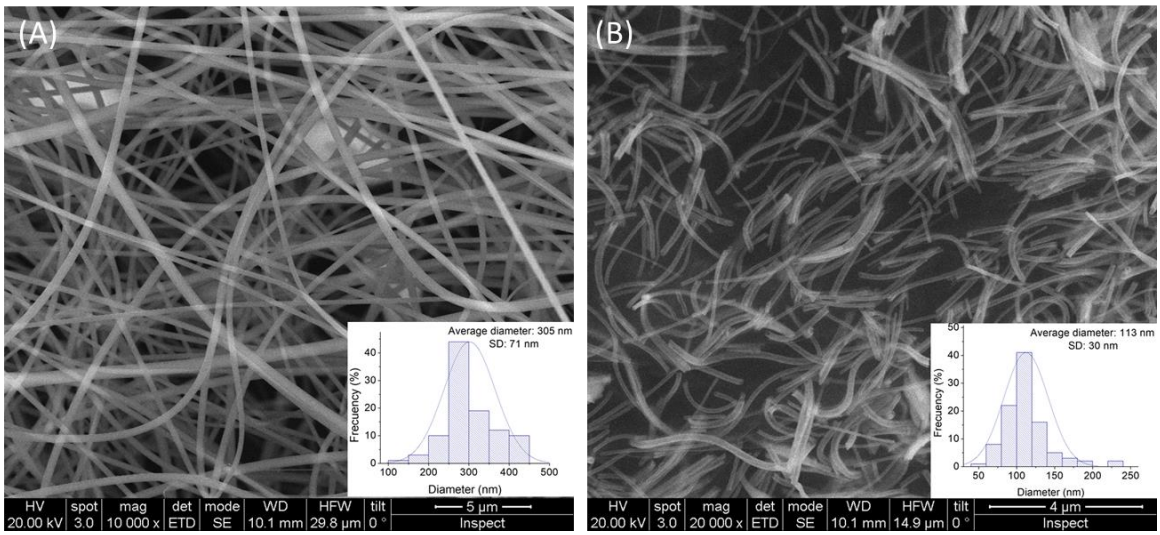

Figure 3: SEM micrographs of (A) nanofibers before calcination process and (B) calcinated CeO_2/NiO nanofibers. Inset images represent the diameter size distribution of the respective figures.

TEM was carried out in order to obtain further information about the morphology of the CeO_2/NiO nanofibers. Figure 4 shows the backbone morphology of the nanofibers containing nanoparticles on the surface, which agrees with reported methods [26]. It was also observed that the nanofibers possess a hollow-like structure in which nanoparticles with an average diameter of 11.2 ± 3 nm are aggregated in the walls, typical of this kind of fibers obtaining from electrospinning method [36]. The formation mechanism of such nanoparticles in the walls of the fiber can be explained due to two combined effects. On the one hand, the solvent evaporation promotes the diffusion of the Ce^{3+}, Ni^{2+} and $(NO_3)^-$ ions in the solution towards the outer part of the formed nanofibers, and in the other hand, the charge accumulation during the applied potential favours the ionic repulsion and thereby the migration of the ionic species as well. Subsequently, during the calcination process both the PVP and the NO_3^- are oxidized to gaseous products, while the Ce^{3+} and Ni^{2+} ions are oxidised forming CeO_2 and NiO crystallites, respectively. These oxide crystallites are re-combined into small nanoparticles which continue the growth in a sintering process to generate the hollow nanofibers [37].

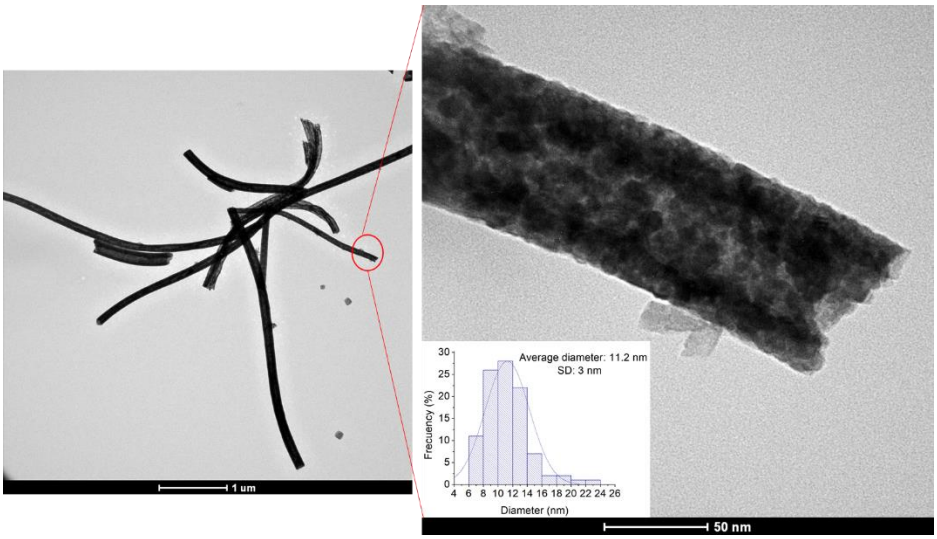

Figure 4: TEM micrograph of the calcinated CeO_2/NiO nanofibers and its respective particle size distribution histogram (inset)

The composition and crystal structure of the CeO_2/NiO nanofibers were characterized by SEM-EDX and XRD. The presence of Ce and Ni elements in calcinated fibers was proved by the EDX spectrum (map of the Figure 3(B)), as presented in Figure 5(A) and its inset. The sample exhibited an atomic percentage of 82% of Ce and 18% of Ni (excluding oxygen), which is similar to the theoretical amount of metals incorporated (85% Ce and 15% Ni). The X-ray diffractogram of CeO_2/NiO nanofibers matches with the reference patterns of CeO_2 (standard ICDD: card no. 00-004-0784) and NiO (standard ICDD: card no. 01-071-4750), as shown in Figure 5(B). The formation of CeO_2 is confirmed by the diffraction peaks at 2θ values of 28.5°, 33.0°, 47.4°, 56.3°, 59.2°, 69.3°, 76.7°, 79.3°, 88.7°, and 95.6° corresponding to (111), (200), (220), (311), (222), (400), (331) (420), (442) and (511) reflections of the cubic crystal CeO_2, respectively. Additionally, the diffraction peaks at 2θ values of 37.2°, 43.1°, 62.6°, 75.8°, 79.3°, 95.3°, 106.4°, and 127.3° correspond to (111), (200), (220), (311), (222), (400), (331) and (422) crystal planes of cubic crystalline NiO, respectively.

Scherrer equation (Equation 1) was used in order to calculate the crystallite size from the width of the peak, this equation relates the crystallite size (τ) with a shape factor (consider in this case K = 0.9), the X-ray wavelength (λ=0.154 nm), the line broadening at half the maximum intensity (β) and the Bragg angle (θ).

$$\tau = \frac{K\lambda}{\beta \cos(\theta)}$$ Equation 1: Scherrer equation

The obtained results show a crystallite size of 8.79 nm, which agrees with the presented results in the TEM analysis.

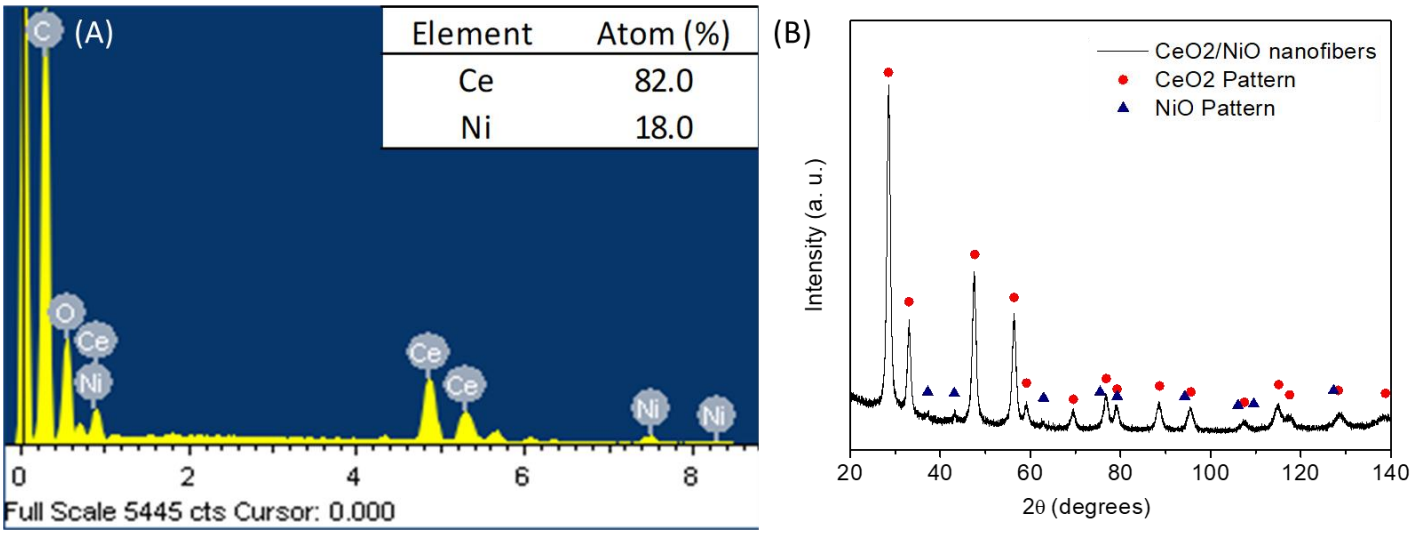

Figure 5: (A) SEM-EDX analysis of the calcinated CeO_2/NiO nanofibers. Insert show the Ce and Ni atomic percentage. (B) XRD patterns of the calcinated CeO_2/NiO calcinated nanofiber.

Furthermore, XPS analysis was perform to study the surface chemical composition of the calcinated CeO_2/NiO nanofibers (Figure 6). Through this technique the presence of cerium and nickel were detected on the surface of the nanofibers, with an atomic percentage of 90% and 10% respectively. The peaks position of Ce $3d_{5/2}$ and the Ni 2p were found at 882.3 eV and 855.6 eV respectively, which correspond to their respective oxides as it can be seen in the Figure 6(A) and Figure 6(B). XPS analysis shows higher Ce atomic surface percentage and lower Ni content compare to the values found in the EDX analysis. This difference might be related to the interaction volume of each technique. XPS spectroscopy, which only interacts with a few atomic layers close to the surface, allows to determine the most superficial composition of the sample. The observed surface Ce enrichment in the fibers can be due the difference of the charge between Ce^{3+} and Ni^{2+} ions in the precursor solution. Ce^{3+} ion, which have higher charge than Ni^{2+}, can diffuse easily outwards due to the evaporation and potential applied, and thereby undergoes to accumulation on the surface of the fibers.

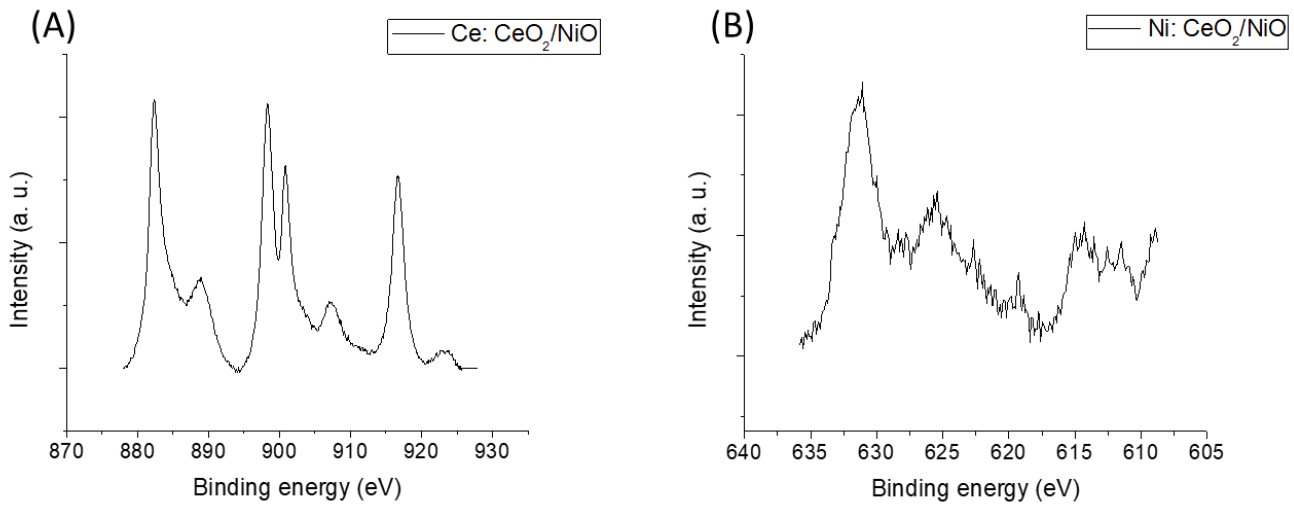

Figure 6: XPS spectra of (A) Ce and (B) Ni in CeO_2/NiO calcinated nanofibers.

Microwave plasma-atomic emission spectroscopy (MP-AES) was used to quantify the bulk amount of atomic Ce and Ni (Table 2) and to compare with the previous characterization methods. The measurements were performed by triplicate with three different wavelengths. The calibration curves are presented in the annex I. Table 2 shows the Ce and Ni atomic percentage of the CeO_2/NiO nanofiber calculated from an average of three MP-AES measurements. The present results agree with the nominal amount of metals incorporated as well as the values found with the EDX analysis.

Table 2: Quantification of Ce and Ni in the calcinated fibers with MP-AES technique

Element	Average concentration (ppm)	Standard deviation	Atomic percentage (%)
Ce	7.00	0.02	84.68
Ni	1.27	0.02	15.32

Further investigation about the reducibility of the CeO_2/NiO nanofiber was carried out by temperature programmed reduction (H_2-TPR) technique. From H_2-TPR profile of in Figure 7, it can be appreciated three main reduction peaks centred at 283 °C, 358 °C and 833 °C. According to the literature [38], the reduction of CeO_2 occurs in two temperature regions: the first one between 300 and 600 °C, which is attributed to the surface reduction process, while the second one between 700 °C and 1000 °C corresponds to the bulk reduction process. It is widely known that CeO_2 can be reduced easily in presence of NiO and consequently, the peaks may shift to lower temperature [35, 36] as it can be appreciated in the Figure 7.

Additionally, two reduction peaks at 400 °C and 550 °C are reported for NiO, corresponding to the overall reduction process: NiO → $Ni^{\delta+}$ → Ni^0 [41]. In this case, only one peak at ca. 400 °C could be identified which suggest that nickel mainly existed in the form of NiO nanoparticles in the CeO_2/NiO nanofibers having strong interaction with the CeO_2 [42].

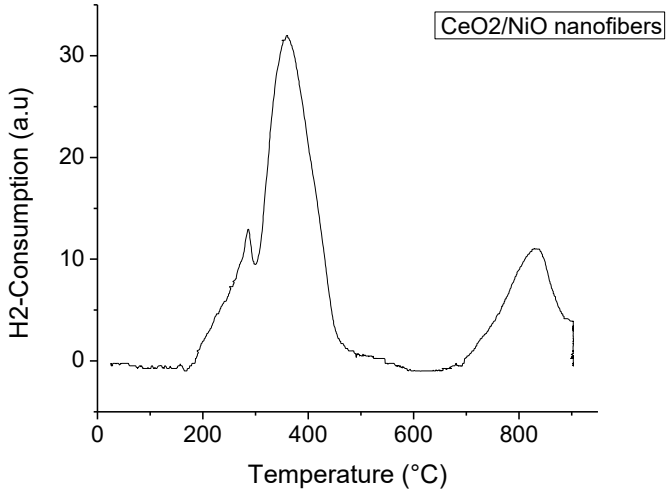

Figure 7: Temperature programmed reduction of CeO_2/NiO calcinated nanofibers.

4.2. CeO_2/NiO/MgO nanofibers

A very similar process used in the previous section was implemented in order to find the best conditions that describe the production of good quality CeO_2/NiO/MgO nanofibers. The electrospinning parameters that allows the stability of the Taylor cone and therefore the production of the high-quality nanofibers were +10/-3 kV of applied voltage, 1 mL/h of feed rate in the internal needle and 0.2 ml/h for the and 25 cm tip-collector distance.

SEM was employed to investigate the general morphology of the CeO_2/NiO/MgO nanofibers. The nanofibers before the calcination process presented an uniform size distribution with an average diameter of 385 ± 78 nm (Figure 8(A)) whereas the calcinated nanofibers showed a smaller average diameter of 175 ± 40 nm (Figure 8(B)). This can be attribute to the elimination of the organic material present in the as-prepared nanofibers during the oxidative calcination process. In order to confirm the success of the calcination process a thermogravimetric analysis (TGA) was performed on the calcinated nanofibers. No significative changes in the sample weight was observed along the temperature range evaluated (25−900 °C), demonstrating the complete removal of the organic PVP matrix.

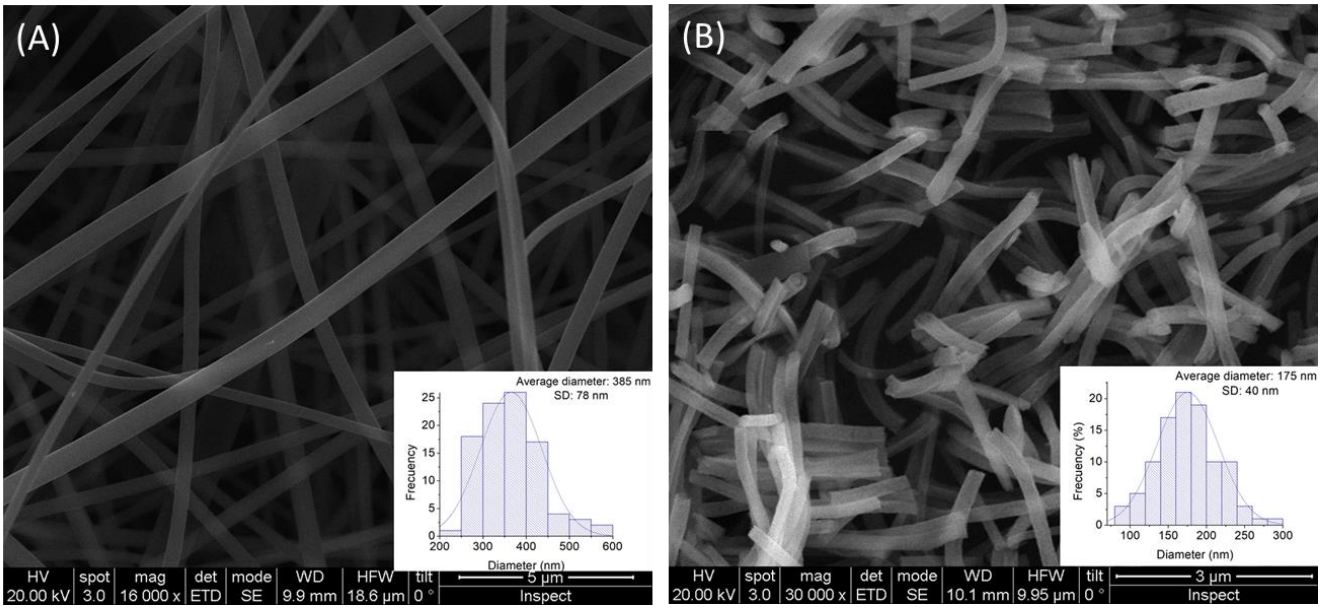

Figure 8: SEM micrographs of the (A) nanofibers before calcination process and (B) calcinated CeO_2/NiO/MgO nanofibers. Insert images represent the diameter size distribution of the respective figures.

TEM was carried out in order to obtain further information about the morphology of the CeO_2/NiO/MgO nanofibers. Figure 9(A) shows the backbone morphology of the nanofibers containing nanoparticles on the surface in agreement with the previous results. The nanofibers possess a hollow-like structure in which nanoparticles with an average diameter of 8.5 ± 1.7 nm are aggregated in the walls. This process is attribute in the same way as the CeO_2/NiO nanofibers regarding the charge of the ion precursor used.

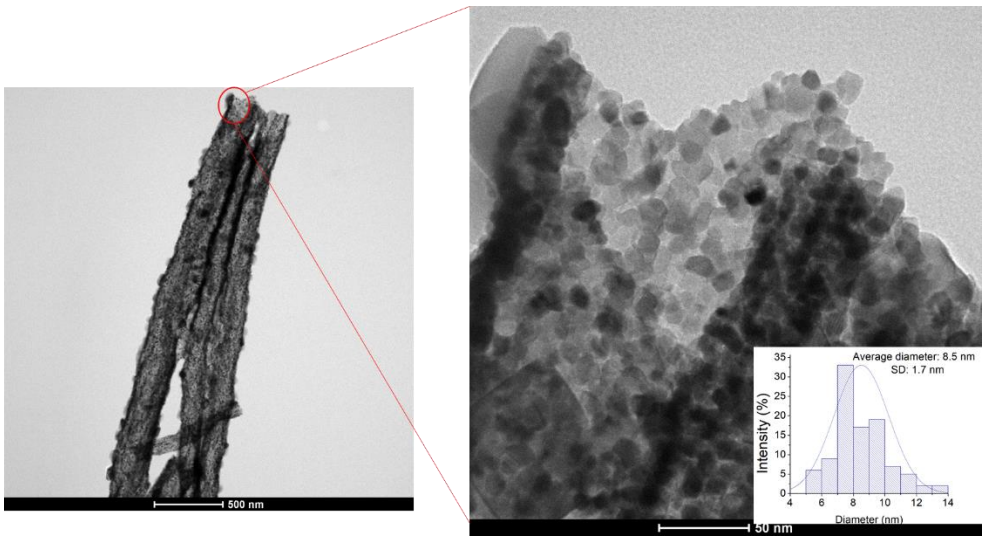

Figure 9: TEM micrograph of the calcinated CeO_2/NiO/MgO nanofibers and its respective particle size distribution histogram (inset)

The composition and crystal structure of the CeO_2/NiO/MgO nanofibers were characterized by EDX and XRD. The presence of Ce, Ni and Mg elements in the calcinated fibers is shown (Figure 10(A) and its inset) in the EDX spectrum taken as a map of the Figure 8(B) .The sample exhibited an atomic percentage of 43.8% of Ce, 35.6% of Mg and 20.6% of Ni (excluding oxygen), which is similar to the nominal amount of metals incorporated (42.5% Ce, 42.5% Mg and 15% Ni). The XRD diffractogram of CeO_2/NiO/MgO nanofibers matches with the reference patterns of CeO_2 (standard ICDD: card no. 00-004-0784) and NiO/MgO (standard ICDD: card no. 00-034-0410), as shown in Figure 10(B). The formation of CeO_2 is confirmed by the diffraction peaks at 2θ values of 28.50, 33.02, 47.42, 56.30, 59.19, 69.30, 76.65, 79.26, 88.69, and 95.58° corresponding to (111), (200), (220), (311), (222), (400), (331) (420), (442) and (511) cubic crystal planes of CeO_2, respectively, while the diffraction peaks at 2θ values of 36.95°, 43.01°, 62.8°, 74.9°, 79.5°, 94.6°, 106.2°, and 110.11° correspond to (111), (200), (220), (311), (222), (400), (331) and (422) respectively with crystal planes of cubic crystalline NiO/MgO pattern.

Scherrer equation (Equation 1) was used in order to calculate the crystallite size from the width of the peak, the obtained results show a crystallite size of 6.5 nm, which agrees with the presented results in the TEM analysis.

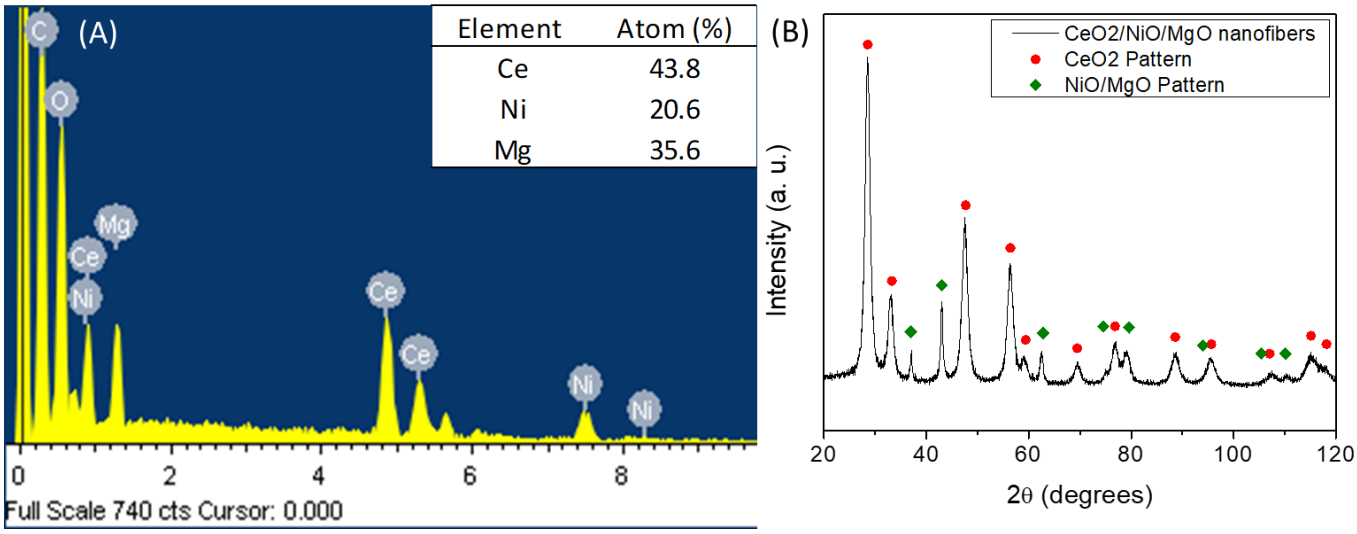

Figure 10: (A) EDX analysis of the calcinated CeO_2/NiO/MgO nanofibers. Insert show the Ce, Ni and Mg atomic ratio. (B) XRD patterns of the calcinated CeO_2/NiO calcinated nanofiber.

Furthermore, XPS analysis was perform to study the surface chemical composition of the calcinated CeO_2/NiO/MgO nanofibers (Figure 11). Through this technique the presence of

cerium, nickel and magnesium were detected on the surface of the nanofibers, with an atomic percentage of 47.51% Ce, 11.43% Ni and 41.06% Mg. The peaks position of Ce $3d_{5/2}$ and the Ni 2p and Mg 1s were found at 882.1 eV , 855.1 eV, and 1304.1 eV, respectively, which correspond to their respective oxides as it can be seen in the Figure 11(A) and Figure 11(B). The obtained atomic percentage values differ from EDX analysis due the enrichment of Ce and Mg in the surface of the fibers. The ion attraction outwards the polymer jet is higher for the Ce^{3+} and Mg^{3+} than Ni^{2+} ions, this can be attributed to the charge difference between those ions, as while higher is the charge, higher is the attraction and therefore there is surface enrichment.

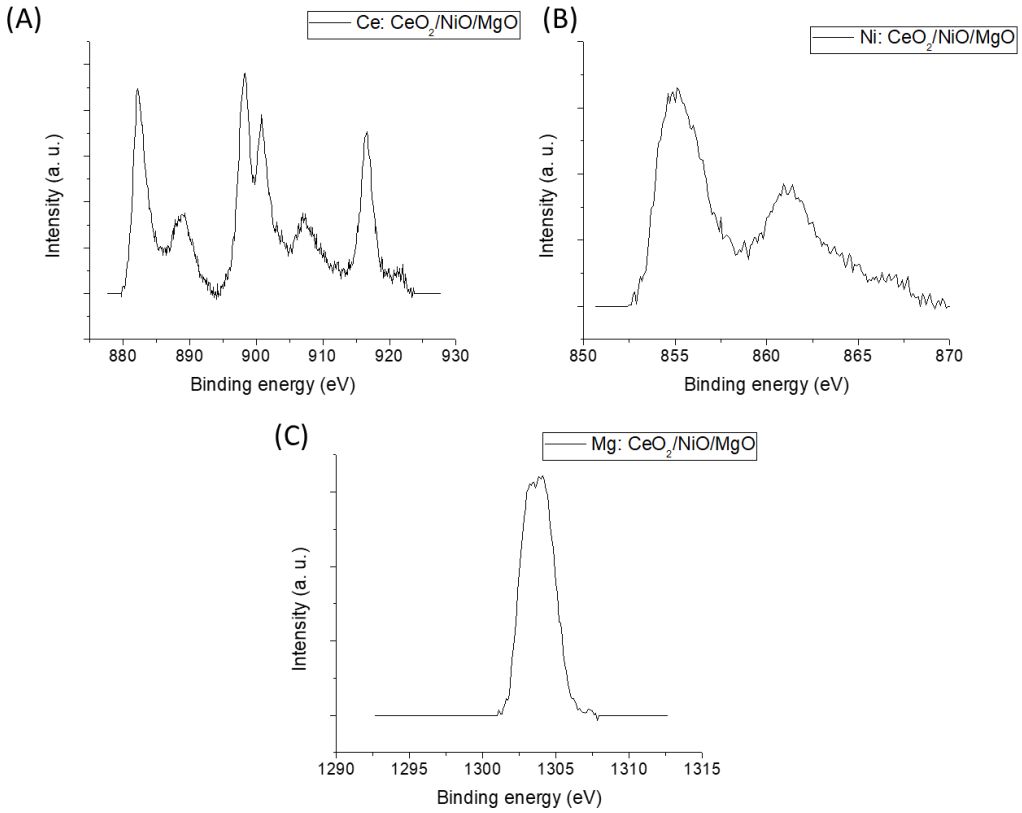

Figure 11: XPS spectra of (A) Ce, (B) Ni and (C) Mg in CeO_2/NiO/MgO calcinated nanofibers

Microwave plasma-atomic emission spectroscopy (MP-AES) was used to quantify the bulk amount of atomic Ce, Ni and Mg (Table 2) and to compare with the previous characterization methods. The measurements were performed by triplicate with three different wavelengths. The calibration curves are presented in the annex II. Table 3 shows the Ce, Ni and Mg atomic percentage of the CeO_2/NiO/MgO nanofiber calculated from an average of three MP-AES

measurements. As the calibration curves were perform just for Ce and Ni, the atomic percentage of Mg was calculated as a difference from the obtained concentration. It was taken into consideration that the nanofibers are composed by the mixture of the CeO2, NiO and MgO according to the TGA results which show no organic material. Comparing bulk (MP-AES) and surface (XPS) results, again there is a decrease in Ni concentration on the surface, as was found for CeO_2/NiO fibers. This fact could be related to the ionic charge of Ni. Ni^{2+} in the precursor solution is less attracted by the applied potential than the other ions, what means a less quantity of this element on the surface of the nanofibers.

Table 3: Quantification of Ce, Ni and Mg in the calcinated fibers with MP-AES technique.

Element	Average concentration (ppm)	Standard deviation	Atomic percentage (%)
Ce	5.80	0.02	40.21
Ni	1.1	0.006	18.20
Mg	-	-	41.59*

4.3. TiO_2 nanofibers doped with Fe_2O_3 nanoparticles

First, Fe_2O_3 nanoparticles were characterize by SEM, by measuring more than 100 particles in several images, it was found an average diameter of 50 ± 10 nm (Figure 12(A)). Figure 12(B) shows the obtained particle size distribution obtained from dynamic light scattering which confirms SEM results, giving a mean diameter of 51.4 ± 0.08 nm. The presence of bigger particles could be due to agglomeration during the analysis.

* Calculated value as a difference from Ce and Ni obtained concentration.

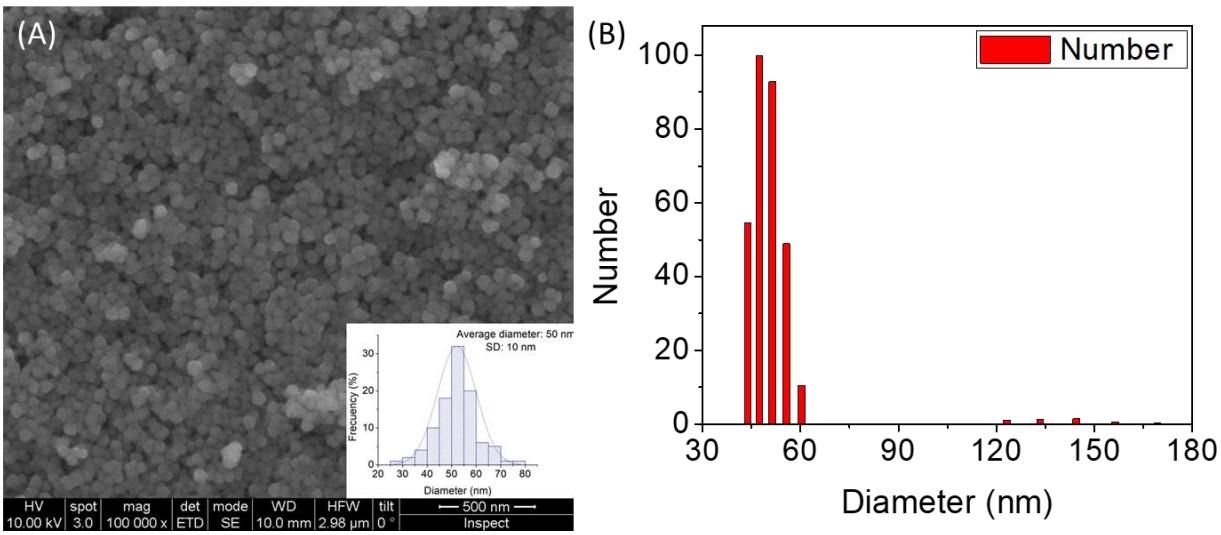

Figure 12: (A) SEM micrograph of Fe_2O_3 nanoparticles with the insert image of particle size distribution histogram and (B) DLS analysis showing particle size distribution (number).

SEM was employed to investigate the general morphology of the Ti-based nanofibers as well. The nanofibers diameter before the calcination process showed two different populations one with a mean value of 57.3 ± 12.6 nm and the other with a mean value of 225.0 ± 27nm (Figure 13(A)). There can be seen particles (red circles in the Figure 13) in some parts of the fibers, especially in the ones with higher diameter that could be attributed to the presence of the Fe_2O_3 . The calcinated nanofibers presented in the Figure 13(B) showed a small average diameter (112.6 ± 25 nm) than the un-calcined ones suggesting the complete polymer elimination. Additionally, a thermogravimetric analysis (TGA) was performed to confirm the success of the calcination process. The results show no significative changes in the sample weight along the temperature range evaluated (25–900 °C), demonstrating the complete removal of the organic PVP matrix.

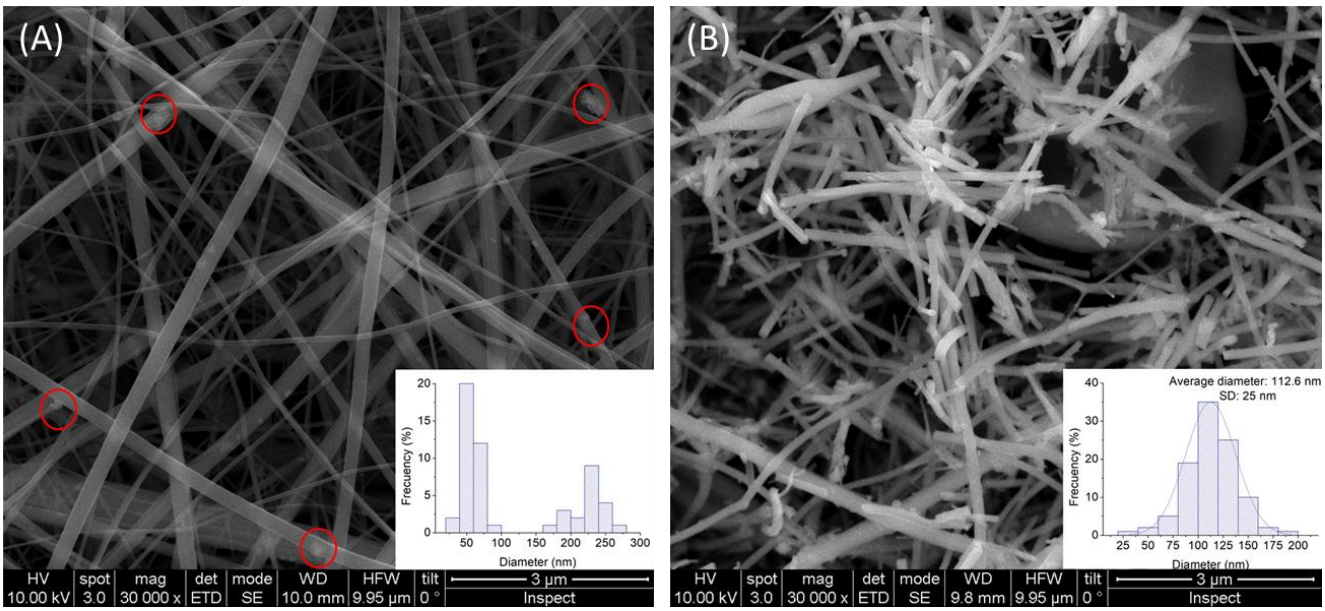

Figure 13:SEM micrographs of the (A) nanofibers before calcination process and (B) calcinated TiO_2 nanofibers doped with Fe_2O_3 nanoparticles. Insert images represent the diameter size distribution of the respective figures.

TEM was carried out in order to obtain further information about the morphology of the TiO_2 nanofibers doped with Fe_2O_3 nanoparticles. Figure 14 shows the backbone morphology of the nanofibers containing both (TiO_2 and Fe_2O_3) nanoparticles on the surface. The nanoparticles marked with the red arrow with approximately 50 nm in size, would correspond to the Fe_2O_3 ones.

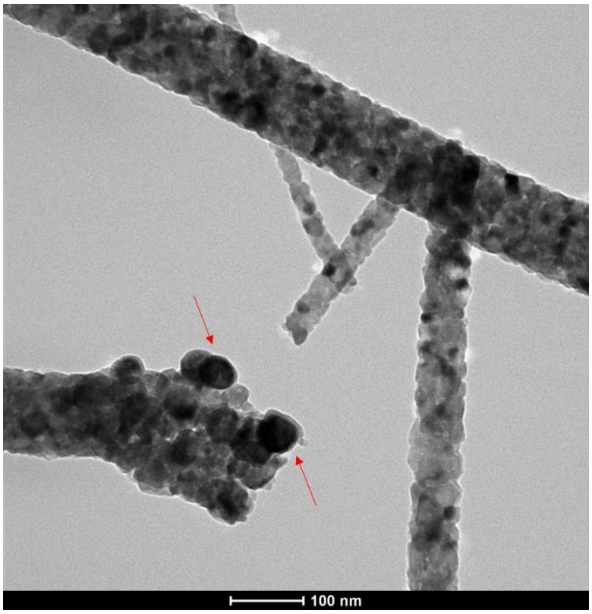

Figure 14: TEM micrograph of the calcinated TiO_2 nanofibers doped Fe_2O_3 NP with insert image of particle size distribution histogram.

SEM-EDX and XRD analysis were performed to identify the Ti and Fe in the TiO_2 nanofibers doped with Fe_2O_3 nanoparticles. According to the Figure 15(A) and its inset, the obtained atomic ratios are smaller than the expected one (91% mol Ti, 9% mol Fe), this can be attribute to the non-homogeneous distribution of the Fe_2O_3 nanoparticles in the sample and the small portion of the sample analysed by SEM (map of the Figure 13(B)).

Titanium dioxide show different crystallinity patterns as rutile (tetragonal), anatase (tetragonal) and brookite (orthorhombic). Among them, rutile and anatase are often used in as photocatalyst, their activity depends on different factors as the structure and the crystallographic orientation [43]. The XRD pattern of TiO_2 nanofibers doped Fe_2O_3 nanoparticles is presented in Figure 15(B). It can be observed the characteristic peaks of both TiO_2 phases, the rutile and anatase according to (standard ICDD: card no. 01-072-4812) and (standard ICDD: card no. 01-084-1286) respectively and the presence with less intensity of the peaks of Fe_2O_3 (standard ICDD: card no. 01-073-2234). The analysis confirms the TiO_2 by the diffraction peaks for the rutile together with the peaks corresponding to anatase crystal planes, also it was confirmed the presence of the characteristic peaks of Fe_2O_3 in a rhombohedral structure. The 2θ values and the crystal planes are shown in the annex II. Scherrer equation (Equation 1) was used in order to calculate the crystallite size from the width of the peak in the TiO_2 corresponding peaks, the obtained results show a crystallite size of 15.5 nm.

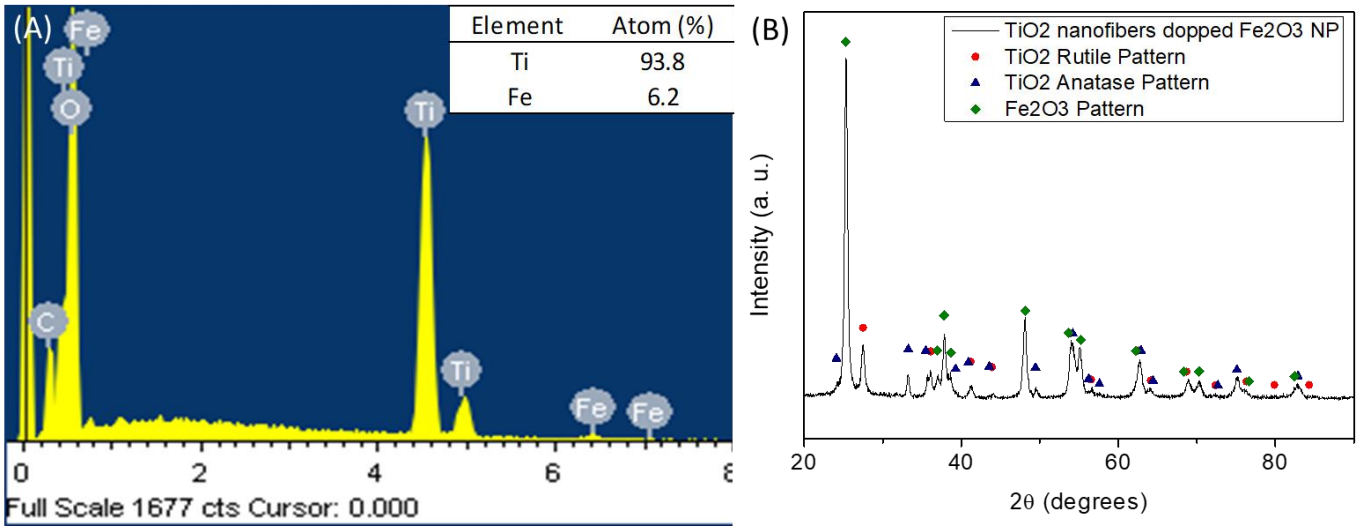

Figure 15: (A) SEM-EDX analysis of the calcinated TiO_2 nanoparticles. Insert show the Ti and Fe atomic ratio. (B) XRD patterns of the calcinated CeO_2/NiO calcinated nanofiber.

Furthermore, XPS analysis was perform to study the surface chemical composition of the calcinated TiO_2 nanofibers doped with Fe_2O_3 nanoparticles (Figure 16). Through this technique the presence of titanium and iron were detected on the surface of the nanofibers, with an atomic percentage of 93.9% Ti and 6.1% Fe. The peaks position of Ti $p_{3/2}$ and Fe 2p a were found at 454.1 eV and 719.0 eV, respectively, which correspond to their respective oxides as it can be seen in the Figure 16(A) and Figure 16(B). The obtained atomic percentage agrees with the value obtained EDX.

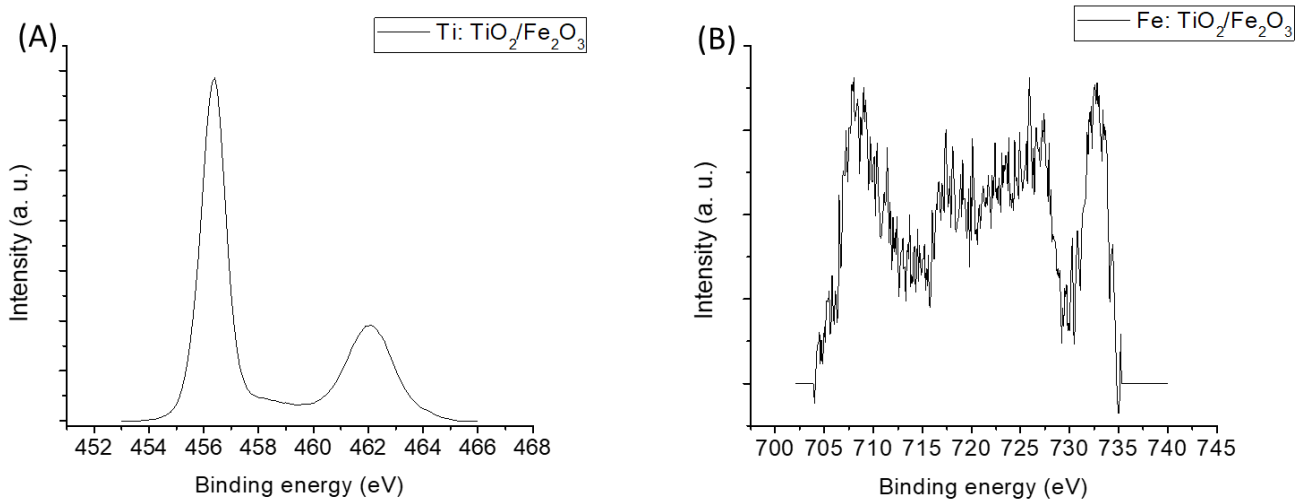

Figure 16: XPS spectra of (A) Ti, and (B) Fe in the TiO_2 calcinated nanofibers doped with Fe_2O_3 nanoparticles.

TiO_2 nanofibers and the TiO_2 nanofibers doped with Fe_2O_3 nanoparticles were studied by UV–Vis spectrometry. Figure 17 shows the UV-Vis diffuse reflectance spectra of the TiO_2 nanofibers and the TiO_2 nanofibers doped with Fe_2O_3 nanoparticles. As it can be observed, the spectra of the TiO_2 nanofibers doped with Fe_2O_3 NP, show a significant enhancement of the light absorption at wavelengths values between 400 nm and 700 nm. This fact can be attributed to the contribution of the Fe_2O_3 nanoparticles which act as a sensitizer for the visible light, and therefore shows an absorption in the visible light region [43,44]. This result is important in order to know proper wavelength range of application in the photocatalytic activity of the material, and it is an advantage for the possibility of use of solar light as the energy supply avoiding the use of ultra-violet light that increment the cost of the process.

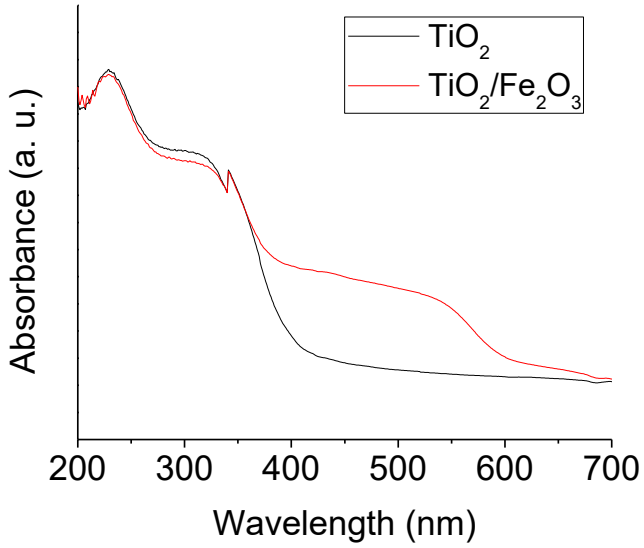

Figure 17: Absorbance spectra of TiO_2 nanofibers (black) and TiO_2 nanofibers doped with Fe_2O_3 nanoparticles (red)

5. Conclusions

Co-precipitation methodology can be implemented to the successful fabrication of CeO_2/NiO and CeO_2/NiO/MgO inorganic nanofibers through the electrospinning process. The best condition of applied voltage of +9/-2 kV for CeO_2/NiO and +10/-3 kV for Ce_2O/NiO/MgO and feed rate of 1 mL/h internal and 0.2 ml/h external, were found in order to obtain the best conditions in which the Taylor's cone was stable for bead-free fibers production. Electrospinning process is also appropriate for the fabrication of TiO_2 nanofibers doped with preformed Fe_2O_3 nanoparticles. By calcination, the organic phase was completely eliminated in all the fibers.

The presented inorganic nanofibers have an average diameter around 113 ± 30 nm, 175 ± 40 nm and 112.6 ± 25 nm for the CeO_2/NiO, CeO_2/NiO/MgO and TiO_2-d-Fe_2O_3 NP, respectively and have nanoparticles as a backbone support of their structure which was confirmed by TEM analysis. The surface and bulk content of each metal was studied trough EDX, and MP-AES confirming that the theoretical values were achieved. Low Ni surface concentration was determined by XPS.

The results obtained in this thesis confirm the applicability of the electrospinning technique for the production of mixed oxide nanofibers with the possibility of the extension of the developed methods to other oxides systems.

6. Future work

With the obtained results in the inorganic nanofibers such as the size, the bulk and surface composition, and the crystal structure, it is proposed their application in catalysis, specifically in the CO_2 methanation and water pollutants removal.

CREG research group from UNIZAR is carrying out tests to study the catalytic behaviour of CeO_2/NiO and CeO_2/NiO/MgO in the CO_2 hydrogenation reaction to produce methanol as a fuel and the comparison with a commercial catalyst.

Following up the degradation of organic pollutants in water by the presence of TiO2 nanofibers doped with Fe_2O_3 nanoparticles. The addition of Fe2O3 makes able the study of the photocatalytic removal of pollutants under visible light. Also, the study of the magnetically recover of the nanofibers due the action of the Fe_2O_3 nanoparticles. Zeolitas' group from the Universidad Tecnologica Nacional, Facultad Regional Cordoba, Argentina is going to perform these experiments.

References

[1] T. Subbiah, G. S. Bhat, R. W. Tock, S. Parameswaran, and S. S. Ramkumar, "Electrospinning of Nanofibers," *J Appl Polym Sci*, vol. 96, pp. 557–569, 2005.

[2] V. Thavasi, G. Singh, and S. Ramakrishna, "Electrospun nanofibers in energy and environmental applications," *Energy Environ. Sci.*, vol. 1, no. 2, p. 205, Jul. 2008.

[3] A. Haider *et al.*, "A comprehensive review summarizing the effect of electrospinning parameters and potential applications of nanofibers in biomedical and biotechnology," *Arab. J. Chem.*, vol. 11, no. 8, pp. 1165–1188, Dec. 2015.

[4] K. Mondal and A. Sharma, "Recent advances in electrospun metal-oxide nanofiber based interfaces for electrochemical biosensing," *RSC Adv.*, vol. 6, no. 97, pp. 94595–94616, Oct. 2016.

[5] N. Wu and Q. Wei, "Inorganic functional nanofibers: processing and applications," *Funct. Nanofibers their Appl.*, pp. 71–91, Jan. 2012.

[6] T. Ludwig, C. Bohr, A. Queraltó, R. Frohnhoven, T. Fischer, and S. Mathur, "Inorganic Nanofibers by Electrospinning Techniques and Their Application in Energy Conversion and Storage Systems," *Semicond. Semimetals*, vol. 98, pp. 1–70, Jan. 2018.

[7] J. Lin, X. Wang, B. Ding, J. Yu, G. Sun, and M. Wang, "Biomimicry via Electrospinning," *Crit. Rev. Solid State Mater. Sci.*, vol. 37, no. 2, pp. 94–114, Apr. 2012.

[8] J. Zeleny, "Instability of Electrified Liquid Surfaces," *Phys. Rev.*, vol. 10, no. 1, pp. 1–6, Jul. 1917.

[9] A. A. Babar and N. Iqbal, "Introduction and Historical Overview," *Electrospinning Nanofabrication Appl.*, pp. 3–20, Jan. 2019.

[10] J. Deitzel, "Electrospinning of polymer nanofibers with specific surface chemistry," *Polymer (Guildf).*, vol. 43, no. 3, pp. 1025–1029, Feb. 2002.

[11] M. H. El-Newehy, S. S. Al-Deyab, E.-R. Kenawy, and A. Abdel-Megeed, "Nanospider Technology for the Production of Nylon-6 Nanofibers for Biomedical Applications," *J. Nanomater.*, vol. 2011, pp. 1–8, 2011.

[12] D. H. Reneker, "Process and apparatus for the production of nanofibers," 2003.

[13] M. Wasim, A. Sabir, M. Shafiq, and T. Jamil, "Electrospinning: A Fiber Fabrication Technique for Water Purification," *Nanoscale Mater. Water Purif.*, pp. 289–308, Jan. 2019.

[14] Z. Li and C. Wang, "Effects of Working Parameters on Electrospinning," Springer Berlin Heidelberg, 2013, pp. 15–28.

[15] N. Bhardwaj and S. C. Kundu, "Electrospinning: A fascinating fiber fabrication technique," *Biotechnol. Adv.*, vol. 28, no. 3, pp. 325–347, 2010.

[16] Z. Li and C. Wang, "Introduction of Electrospinning," Springer, Berlin, Heidelberg, 2013, pp. 1–13.

[17] R. A. Damodar, S.-J. You, and H.-H. Chou, "Study the self cleaning, antibacterial and photocatalytic properties of TiO 2 entrapped PVDF membranes," *J. Hazard. Mater.*, vol. 172, pp. 1321–1328, 2009.

[18] R. Vasita and D. S. Katti, "Nanofibers and their applications in tissue engineering.," *Int. J. Nanomedicine*, vol. 1, no. 1, pp. 15–30, 2006.

[19] S.-T. Hwang, Y.-B. Hahn, K.-S. Nahm, and Y.-S. Lee, "Preparation and characterization of poly(MSMA-co-MMA)-TiO2/SiO2 nanocomposites using the colloidal TiO2/SiO2 particles via blending method," *Colloids Surfaces A Physicochem. Eng. Asp.*, vol. 259, no. 1–3, pp. 63–69, May 2005.

[20] S. Wen, M. Liang, R. Zou, Z. Wang, D. Yue, and L. Liu, "Electrospinning of palladium/silica nanofibers for catalyst applications," *RSC Adv.*, vol. 5, no. 52, pp. 41513–41519, May 2015.

[21] A. Barhoum, R. Rasouli, M. Yousefzadeh, H. Rahier, and M. Bechelany, "Nanofiber Technology: History and Developments," in *Handbook of Nanofibers*, Cham: Springer International Publishing, 2018, pp. 1–42.

[22] D. L. and and Y. Xia*, "Fabrication of Titania Nanofibers by Electrospinning," 2003.

[23] J. Moon, J.-A. Park, S.-J. Lee, T. Zyung, and I.-D. Kim, "Pd-doped TiO2 nanofiber networks for gas sensor applications," *Sensors Actuators B Chem.*, vol. 149, no. 1, pp. 301–305, Aug. 2010.

[24] M. Y. Song, D. K. Kim, K. J. Ihn, S. M. Jo, and D. Y. Kim, "Electrospun TiO $_2$ electrodes for dye-sensitized solar cells," *Nanotechnology*, vol. 15, no. 12, pp. 1861–1865, Dec. 2004.

[25] J. Yerasi, "Electrospinning of Ceria and Nickel Oxide Nanofibers," *Theses*, Aug. 2014.

[26] Y. Liu, X. Sun, Z. Zhou, and Y. Lei, "Electrospun Ce–Ni–O composite nanofibers for highly selective propane detection at high temperature based on its rapid reaction kinetics," *J. Mater. Chem. A*, vol. 2, no. 34, p. 14038, Jun. 2014.

[27] W. Wei and G. Jinlong, "Methanation of carbon dioxide: an overview," *Front. Chem. Sci. Eng.*, vol. 5, no. 1, pp. 2–10, Mar. 2011.

[28] N. H. Elsayed, D. Maiti, B. Joseph, and J. N. Kuhn, "Precious Metal Doped Ni–Mg/Ceria–Zirconia Catalysts for Methane Conversion to Syngas by Low Temperature Bi-reforming," *Catal. Letters*, vol. 148, no. 3, pp. 1003–1013, Mar. 2018.

[29] B. Ding, C. K. Kim, H. Y. Kim, M. K. Seo, and S. J. Park, "Titanium dioxide

nanofibers prepared by using eletrospinning method," *Fibers Polym.*, vol. 5, no. 2, pp. 105–109, Jun. 2004.

[30] I. Tlili and T. A. Alkanhal, "Nanotechnology for water purification: electrospun nanofibrous membrane in water and wastewater treatment," *J. Water Reuse Desalin.*, Jan. 2019.

[31] H. Wang *et al.*, "Magnetically separable iron oxide nanostructures-TiO2 nanofibers hierarchical heterostructures: controlled fabrication and photocatalytic activity," *New J. Chem.*, vol. 35, no. 9, p. 1795, Sep. 2011.

[32] N. Sobti, A. Bensouici, F. Coloma, C. Untiedt, and S. Achour, "Structural and photoelectrochemical properties of porous TiO2 nanofibers decorated with Fe2O3 by sol-flame," *J. Nanoparticle Res.*, vol. 16, no. 8, p. 2577, Aug. 2014.

[33] D. Nurwaha, W. Han, and X. Wang, "Effects of processing parameters on electrospun fiber morphology," *J. Text. Inst.*, vol. 104, no. 4, pp. 419–425, Apr. 2013.

[34] T. J. Sill and H. A. von Recum, "Electrospinning: Applications in drug delivery and tissue engineering," *Biomaterials*, vol. 29, no. 13, pp. 1989–2006, May 2008.

[35] † Silke Megelski, † Jean S. Stephens, ‡ and D. Bruce Chase, and † John F. Rabolt*, "Micro- and Nanostructured Surface Morphology on Electrospun Polymer Fibers," 2002.

[36] C. Thiabdokmai, A. Tangtrakarn, S. Promsuy, P. Ngiewlay, and C. Mongkolkachit, "Templateless Synthesis and Characterization of Hollow Gadolinium Doped Cerium Oxide Nanofibers by Electrospinning," *Adv. Mater. Sci. Eng.*, vol. 2014, pp. 1–10, Jun. 2014.

[37] Q. CUI, X. DONG, J. WANG, and M. LI, "Direct fabrication of cerium oxide hollow nanofibers by electrospinning," *J. Rare Earths*, vol. 26, no. 5, pp. 664–669, Oct. 2008.

[38] G. R. Rao, "Influence of metal particles on the reduction properties of ceria-based materials studied by TPR," *Bull. Mater. Sci.*, vol. 22, no. 2, pp. 89–94, Apr. 1999.

[39] J. Wang *et al.*, "Effects of Ni-Doping of Ceria-Based Materials on Their Micro-Structures and Dynamic Oxygen Storage and Release Behaviors," *Catal. Letters*, vol. 140, no. 1–2, pp. 38–48, Nov. 2010.

[40] D. Srinivas, C. V. V. Satyanarayana, H. S. Potdar, and P. Ratnasamy, "Structural studies on NiO-CeO2-ZrO2 catalysts for steam reforming of ethanol," *Appl. Catal. A Gen.*, vol. 246, no. 2, pp. 323–334, Jun. 2003.

[41] L. WANG, H. LIU, Y. LIU, Y. CHEN, and S. YANG, "Influence of preparation method on performance of Ni-CeO2 catalysts for reverse water-gas shift reaction," *J. Rare Earths*, vol. 31, no. 6, pp. 559–564, Jun. 2013.

[42] T. Odedairo, J. Chen, and Z. Zhu, "Metal–support interface of a novel Ni–CeO2 catalyst for dry reforming of methane," *Catal. Commun.*, vol. 31, pp. 25–31, Jan. 2013.

[43] T. Luttrell, S. Halpegamage, J. Tao, A. Kramer, E. Sutter, and M. Batzill, “Why is anatase a better photocatalyst than rutile? - Model studies on epitaxial TiO2 films,” *Sci. Rep.*, vol. 4, no. 1, p. 4043, May 2015.

[44] H. Liu and L. Gao, “Preparation and Properties of Nanocrystalline alpha-Fe2O3-Sensitized TiO2 Nanosheets as a Visible Light Photocatalyst,” *J. Am. Ceram. Soc.*, vol. 89, no. 1, pp. 370–373, Jan. 2006.

Annex I. Microwave plasma – atomic emission spectrometry calibration curves

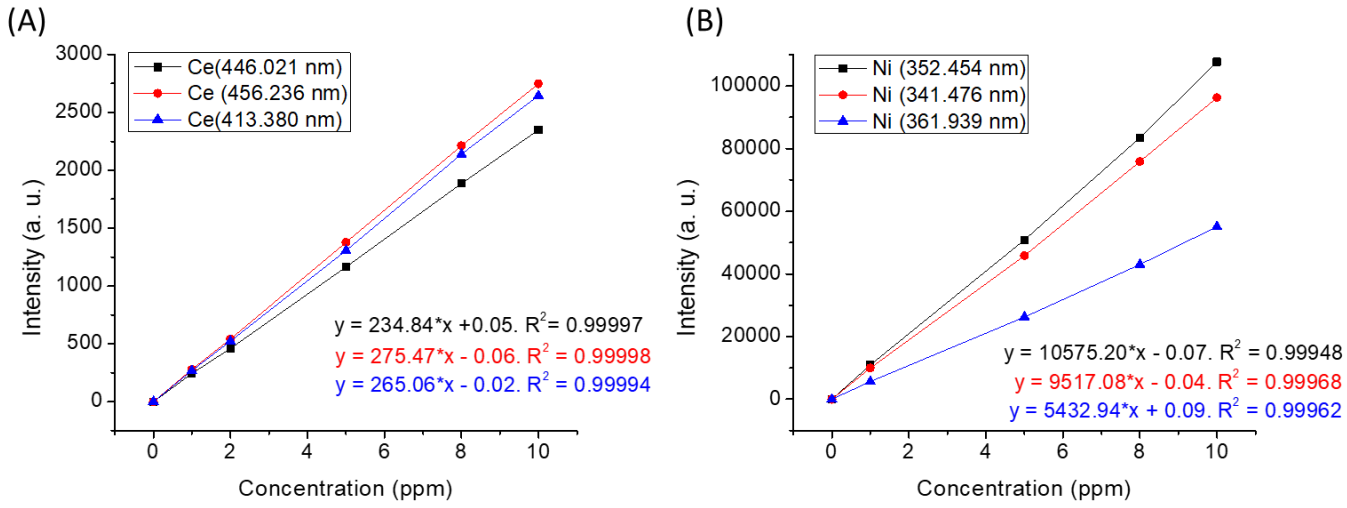

MP-AES calibration curve of (A) Cerium pattern and (B) Nickel pattern.

Annex II. Characteristic crystal planes of TiO_2 rutile and anatase and Fe_2O_3

TiO_2 Rutile		TiO_2 anatase		Fe_2O_3	
2θ (°)	Crystal planes	2θ (°)	Crystal planes	2θ (°)	Crystal planes
27.4	(110)	25.3	(101)	24.2	(012)
36.0	(101)	37.0	(103)	33.2	(104)
39.1	(220)	37.8	(004)	35.6	(110)
41.2	(111)	38.6	(112)	39.3	(006)
43.9	(210)	48.1	(200)	40.9	(113)
54.3	(211)	53.9	(105)	43.5	(202)
56.5	(220)	55.1	(211)	49.5	(024)
62.8	(002)	62.2	(213)	54.1	(116)
63.9	(310)	68.8	(204)	56.2	(211)
65.4	(221)	70.3	(116)	57.5	(122)
68.9	(301)	74.1	(220)	57.7	(018)
69.8	(112)	75.1	(007)	62.5	(214)
72.3	(311)	76.1	(215)	64	(300)
74.2	(320)	80.9	(301)	66.1	(125)
76.5	(202)	82.2	(008)	69.6	(208)
79.8	(212)	82.8	(303)	72	(1010)
82.2	(321)			72.3	(119)
84.1	(400)			75.2	(217)
				75.5	(220)
				77.8	(306)
				78.8	(223)
				79.5	(131)
				80.6	(312)